

Interaction of the early 3d transition metals Sc, Ti, V, and Cr with N₂: An *ab initio* study

Stavros Kardahakis, Constantine Koukounas, and Aristides Mavridis^{a)}

Laboratory of Physical Chemistry, Department of Chemistry,
National and Kapodistrian University of Athens, P.O. Box 64 004, 15710 Zografou, Athens, Greece

(Received 28 November 2005; accepted 19 January 2006; published online 13 March 2006;
publisher error corrected 20 March 2006)

The interaction of the early 3d transition elements $M = \text{Sc, Ti, V, and Cr}$ with $\text{N}_2(X^1\Sigma_g^+)$ has been studied by coupled-cluster and multiconfigurational techniques in conjunction with quantitative basis sets. We investigated both triatomic (MN_2) and tetratomic (M_2N_2) species but focused mainly on high-spin linear and T-shaped triatomics. The lowest bound states of $\text{ScN}_2(^4B_1)$, $\text{TiN}_2(^5\Delta)$, and $\text{VN}_2(^6\Sigma^+)$ correlate to the first excited state of the M atom, with $M-\text{N}_2$ binding energies (D_e) of 24, 14, and 8 kcal/mol, respectively. In CrN_2 , the first bound state $^7\Pi$ correlates to the sixth excited state of the Cr atom (7P) with $D_e = 27$ kcal/mol. The $M-\text{N}_2-M$ bond strength of high-spin linear tetratomics is twice as large the binding energy of the corresponding $M-\text{N}_2$ linear triatomics, $M = \text{Sc, Ti, V, and Cr}$. © 2006 American Institute of Physics. [DOI: 10.1063/1.2174000]

I. INTRODUCTION

Recently, we examined the interaction of the first four 3d transition metal atoms Sc, Ti, V, and Cr with carbon monoxide $\text{CO}(X^1\Sigma^+)$ by coupled-cluster and multireference variational methods.¹ It was concluded that the ground state binding energies (D_0) of $\text{ScCO}(\tilde{X}^4\Sigma^-)$, $\text{TiCO}(\tilde{X}^5\Delta)$, $\text{VCO}(\tilde{X}^6\Sigma^+)$, and $\text{CrCO}[\tilde{X}^7A'(^7\Sigma^+)]$ are 36, 27, 18, and 2 kcal/mol, respectively. Note that the D_0 values of ScCO , TiCO , and VCO refer to the end products $\text{Sc}(a^4F; 4s^13d^2)$, $\text{Ti}(a^5F; 4s^13d^3)$, and $\text{V}(a^6D; 4s^13d^4) + \text{CO}(X^1\Sigma^+)$, i.e., with respect to the first excited state of the metal atoms. The relatively strong $M-\text{CO}$ attractive interactions, at least for the first three MCO species, can be attributed to a rather weak σ charge transfer from CO to the metal and a stronger “ π back donation” from the M atom(s) to CO due to $3d_\pi(M)-2p_\pi(\text{CO})$ conjugation. However, all MCO states correlating to the ground state metal atoms were found to be repulsive.

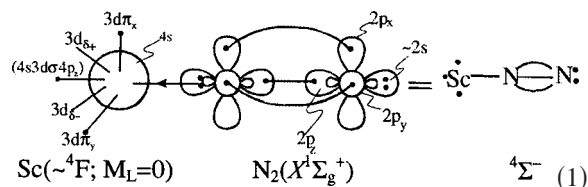
Our motivation for the present report stems from the striking similarity between the electronic structure of the CO and N_2 molecules, the general interest in $M-\text{N}_2$ interactions,² and the almost complete lack of *ab initio* and experimental data on the MN_2 species.

The molecules VN_2 , CrN_2 , and ScN_2 have been experimentally detected only recently by matrix IR spectroscopy.^{3,4} The same authors have also performed density functional theory (DFT) calculations on the ground and certain excited states of VN_2 , CrN_2 , and ScN_2 ; specifically, DFT(BPL)/6-311+ G^* on VN_2 and CrN_2 (Ref. 3) and DFT(BP86)/6-31+ G^* on ScN_2 .⁴ DFT(B3LYP)/6-311+ $G(2d,p)$ calculations on MN_2 , $M = \text{Sc-Cu}$ have also been published recently by Pilme *et al.*⁵ To our knowledge, no *ab initio* calculations at

any level have ever been reported in the literature on ScN_2 , TiN_2 , VN_2 , or CrN_2 .

The ground state terms of Sc, Ti, V, and Cr are $^2D(4s^23d^1)$, $^3F(4s^23d^2)$, $^4F(4s^23d^3)$, and $^7S(4s^13d^5)$, respectively.⁶ The axial interaction of a closed shell strongly bound molecule of cylindrical symmetry, like N_2 in its ground state ($X^1\Sigma_g^+$), with any of the above ground state metal atoms is expected to produce repulsive $M-\text{N}_2$ molecular states. For instance, the $\text{Sc}(^2D)+\text{N}_2$ linear approach gives rise to $^2\Sigma^+$, $^2\Pi$, and $^2\Delta$ states of repulsive character, very similar in nature to those of $\text{Sc}(^2D)+\text{CO}(X^1\Sigma^+)$.¹ Similarly, a side-on attack of a ground state M atom to N_2 (C_{2v} symmetry) is not expected to lead to attractive interactions.

Considering now our experience with the MCO molecules,¹ the situation becomes more interesting if the Sc, Ti, and V atoms are promoted to their first excited state, namely, $^4F(4s^13d^2)$, $^5F(4s^13d^3)$, and $^6D(4s^13d^4)$, 1.427, 0.806, and 0.245 eV higher, respectively.⁶ Let us take again as an example the 4F state of Sc interacting in a linear fashion (end on) with $\text{N}_2(X^1\Sigma_g^+)$; under this geometry molecular states of $^4\Sigma^-$, $^4\Pi^\pm$, $^4\Delta^\pm$, and $^4\Phi^\pm$ symmetries are obtained, three of which are doubly degenerate, i.e., a total of seven states. According to the analysis of Ref. 1, the $^4\Sigma^-$ should be the lowest among the linear states. The following valence-bond-Lewis (vbL) diagram captures the essence of the $\text{Sc}-\text{N}_2^4\Sigma^-$ interaction.

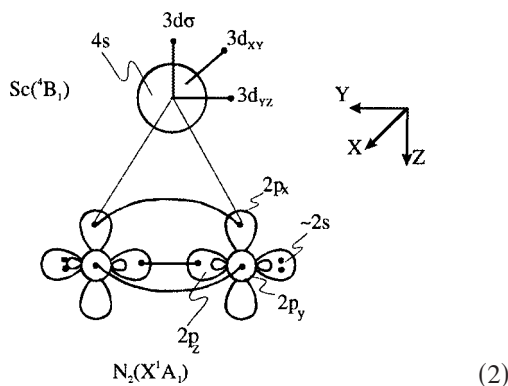


According to diagram (1) an attractive interaction is clearly plausible through a σ charge transfer from a $\sigma(2s2p_z)$ (N_2) hybrid orbital to the $4s$ orbital of Sc, with the concomitant assistance of $(3d\pi_x^1, 3d\pi_y^1)-(2p\pi_x^2, 2p\pi_y^2)$ charge

^{a)}Electronic mail: mavridis@chem.uoa.gr

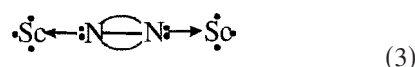
conjugation (for details see Ref. 1). Analogous diagrams can be drawn for the ${}^4\Pi$, ${}^4\Delta$, and ${}^4\Phi$ linear states.

Lowering the symmetry to C_{2v} (side-on approach), the three doubly degenerate ${}^4\Pi^\pm$, ${}^4\Delta^\pm$, and ${}^4\Phi^\pm$ states split into ${}^4B_1 + {}^4B_2$, ${}^4A_1 + {}^4A_2$, and ${}^4B_1 + {}^4B_2$ components, respectively; ${}^4\Sigma^-$ transforms accordingly to 4A_2 . A 4B_1 state is shown schematically in diagram (2).



Some of these C_{2v} states are examined in the present work (*vide infra*).

Despite the obvious structural similarities between N_2 and CO molecules, the lower symmetry of the latter ($C_{\infty v}$ vs $D_{\infty h}$) induces some important differences. First, the $X^1\Sigma^+$ state of CO has a dipole moment $\mu_e = 0.1222$ D,⁷ with its negative end residing on the carbon atom, and second, the $D_{\infty h}$ symmetry of N_2 allows for an amphidextrous bonding behavior. Indeed, observing diagram (1), it is clear that a second Sc atom can attach itself to the “right” N_2 end of $ScN_2^4\Sigma^-$ state, thus creating a high-spin ${}^7\Sigma_u^+$ state of linear geometry, viz.,



It is expected that the second Sc atom should enter with approximately equal binding energy as compared to the first. Indeed, our calculations show that these “acetylene-like” structures have an atomization energy with respect to N_2 , about twice as large as that of the corresponding MN_2 molecule.

It is obvious that the discussion above can be carried over to the interaction of Ti and V atoms with N_2 ; Cr does not conform to these ideas due to the different character of its ground ${}^7S(4s^13d^5)$ and first excited ${}^5S(4s^13d^5)$ states (but see below).

Within this spirit we have performed highly correlated coupled-cluster and multireference calculations in conjunction with large and very large basis sets. We examined the ground and some low-lying excited states of the ScN_2 , TiN_2 , VN_2 , and CrN_2 species. In addition, the relative stability and bonding of the high-spin tetratomics Sc_2N_2 , Ti_2N_2 , V_2N_2 , and Cr_2N_2 have been also investigated. We report equilibrium geometries, energetics, harmonic frequencies, and dipole moments. For selected states of the MN_2 triatomics, we have also computed potential energy profiles (PEPs) with respect to $M+N_2(X^1\Sigma_g^+)$.

II. BASIS SETS AND METHODS

For all calculations the averaged atomic natural orbitals (ANO) basis sets of Bauschlicher⁸ (B) $21s16p9d6f4g$ (Sc, Ti) and $20s15p10d6f4g$ (V, Cr) were used. For the N atom Dunning’s⁹ correlation consistent basis of quadruple cardinality augmented with a series of diffuse functions aug-cc-pVQZ = $13s7p4d3f2g$ (AQZ) was employed. Both sets were generally contracted to $[7s6p4d3f2g/M6s5p4d3f2g/N]$, numbering 244 ($M+2N$) spherical Gaussians. To monitor our results with respect to the basis set size, the recently developed extended correlation consistent basis sets of quintuple quality by Peterson¹⁰ (P) for the 3d transition metal atoms cc-pV5Z = $28s20p12d4f3g2h1i$ were employed, combined with the aug-cc-pV5Z = $15s9p5d4f3g2h$ for N.⁹ Both sets were generally contracted to $[9s8p6d4f3g2h1i/M7s6p5d4f3g2h/N] \equiv 5Z$. Finally, the $M-5Z$ sets were augmented by a series of $2s+2p+2d+1f+1g+1h+1i$ weighted core functions for the $\sim 3s^23p^6$ semi-core electrons of M , giving rise to the contracted $[11s10p8d5f4g3h2i/M7s6p5d4f3g2h/N] \equiv C5Z$ set amounting to 465 ($M+2N$) spherical Gaussians. These very large C5Z sets were used only for the lowest linear structures of $ScN_2({}^4\Sigma^-)$, $TiN_2({}^5\Delta)$, and $VN_2({}^6\Sigma^+)$.

Our numerical results were obtained mainly by the single reference coupled-cluster (CC) method, i.e., restricted HartreeFock+single+double excitations+noniterative connected triples=RCCSD(T), as implemented in the MOLPRO suite of codes.^{11,12} For the “ground” linear states (but see below), core ($3s^23p^6$)/valence-correlation effects and scalar relativity through the second order Douglas-Kroll-Hess¹³ (DKH2) approximation were taken into account using both the Bauschlicher ANO (Ref. 8) and Peterson basis sets.¹⁰ Notice that the ANO basis sets were not supplemented by specially tuned core functions as in the case of the Peterson basis. For all other states examined, our calculations are limited to the “simple” valence-correlation level. In the DKH2 calculations the ANO(M)+AQZ(N) sets were used uncontracted, whereas for the (C)5Z sets of M s, the Peterson’s recommendations were followed,¹⁰ uncontracting at the same time the A5Z set of nitrogen. Valence calculations with relativistic corrections are referred to as RCCSD(T)+DKH2 and as C-RCCSD(T), C-RCCSD(T)+DKH2 when core and core+relativity effects are taken into consideration, respectively.

For almost all states of triatomics, complete active space self-consistent field+single+double replacements (CASSCF+1+2=MRCI) calculations were performed around equilibrium geometries for reasons of comparison and for obtaining more sensible MRCI atomic Mulliken populations. The reference space is built by allotting the 3, 4, 5, and 6 “valence” electrons of Sc, Ti, V, and Cr atoms, respectively, to the six $4s3d$ M orbitals, whereas all our CASSCF wave functions obey axial symmetry conditions. Note that in the MRCI calculations the basis set on N is of the plain quadruple quality, cc-pVQZ (QZ). The single and double excitations out of the CASSCF reference functions include of course all valence electrons of the MN_2 species, i.e., 13, 14, 15, and 16, for ScN_2 , TiN_2 , VN_2 , and CrN_2 . The internally contracted MRCI spaces range from about 400 000 ($VN_2; {}^6\Sigma^+$) to

TABLE I. Absolute energies (E_h) and separation energies (cm⁻¹) of the ground and first excited states of Sc, Ti, V, and Cr.

Method/basis set ^a	Sc(a^2D)	Sc($a^4F \leftarrow a^2D$)	Ti(a^3F)	Ti($a^5F \leftarrow a^3F$)	V(a^4F)	V($a^6D \leftarrow a^4F$)	Cr(a^7S)
RCCSD(T)/ANO	-759.779 26	13 188	-848.464 70	7435	-942.966 73	2388	-1043.464 75
RCCSD(T)/5Z	-759.779 98	12 212	-848.465 90	7468	-942.968 85	2399	-1043.467 55
RCCSD(T)+DKH2/ANO	-763.325 61	14 205	-852.799 74	8630	-948.216 68	3784	-1049.760 98
RCCSD(T)+DKH2/5Z	-763.325 80	14 152	-852.800 37	8623	-948.217 95	3777	-1049.762 86
C-RCCSD(T)/ANO	-760.068 27	12 111	-848.780 11	5782	-943.303 53	829	-1043.822 38
C-RCCSD(T)/C5Z	-760.134 23	11 591	-848.851 92	5466	-943.381 23	664	-1043.906 03
C-RCCSD(T)+DKH2/ANO	-763.664 98	12 598	-853.169 78	7098	-948.609 07	2475	-1050.173 66
C-RCCSD(T)+DKH2/C5Z	-763.680 53	12 565	-853.186 51	6667	-948.630 56	2079	-1050.201 65
Expt. ^b		11 510		6501		1977	

^aDKH2 refers to scalar relativistic corrections through the Douglas-Kroll-Hess second order approximation.

^bReference 6.

800 000(TiN₂; ³ Δ) configuration functions; for the ⁷ Π state of CrN₂, the icMRCI space rises to 1 750 000 configurations because of the inclusion of three $4p$ orbitals in the active space. Size-nonextensivity effects, the most serious drawback of the MRCI method, were ameliorated by using the supermolecule approach and the Davidson (Q) correction in the calculation of dissociation energies.

III. THE Sc, Ti, V, AND Cr ATOMS

Table I lists the total and separation CC energies between the ground and first excited states of Sc, Ti, V, and Cr in the ANO (Ref. 8) (B) and (C)5Z¹⁰ (P) basis sets. The $4s^23d^q \rightarrow 4s^13d^{q+1}$ promotion energy is of obvious importance, since attractive $M+N_2(X^1\Sigma_g^+)$ interactions correlate to the first excited state of the Sc, Ti, and V atoms as was previously discussed. The following conclusions can be drawn from the data of Table I.

Both basis sets (B, P) behave similarly at the RCCSD(T) or RCCSD(T)+DKH2 level: excitation energies are overestimated significantly, particularly when including DKH2 relativistic effects. Including the $3s^23p^6$ semicore electrons [C-RCCSD(T)], the excitation energies of Ti and V are severely underestimated, but that of Sc is in excellent agreement with experiment at the C-RCCSD(T)/C5Z level, perhaps fortuitously. Moving at the next level of theory, i.e., including DKH2 effects, we can claim that the $4s^23d^q \rightarrow 4s^13d^{q+1}$ splittings are in very good agreement with the experimental results, particularly at the C-RCCSD(T)+DKH2/C5Z level, the largest discrepancy being about $1000 \text{ cm}^{-1} \{ \text{Sc}(a^4F \leftarrow a^2D) \}$.

At the RCCSD(T)/AQZ level, the total energy (E_e), binding energy (D_e), bond length (r_e), and harmonic frequency (ω_e) of $N_2(X^1\Sigma_g^+)$ are (experimental values in parenthesis) $-109.407\,243 E_h$, 224.0 (228.4) kcal/mol, 1.1005 (1.0977) Å, and 2354 (2358.6) cm⁻¹, respectively.

IV. RESULTS AND DISCUSSION

Table II collects all our numerical values on the MN_2 species, $M=\text{Sc, Ti, V, and Cr}$; potential energy profiles (slices of potential energy surfaces) at the RCCSD(T)/ANO+AQZ level are presented in Figs. 1–4. We report the total energies, dissociation energies [D_e and $D_0 = D_e - \text{ZPE} = D_e - \frac{1}{2}[\sum_i^4 \omega_i(MN_2) - \omega(N_2; X^1\Sigma_g^+)]$], geometries

r_{M-N}, r_{N-N} , separation energies T_e , harmonic frequencies $\{\omega_i\}$, and dipole moments μ_e in different levels of theory.

A. ScN₂

The three doublets ² $\Pi, ^2\Delta$, and ² Σ^+ correlating to the ground state products $\text{Sc}(^2D)+N_2(X^1\Sigma_g^+)$ are, as expected, repulsive, see Fig. 1. The ordering ² $\Pi < ^2\Delta < ^2\Sigma^+$ is identical to those of ScCO,¹ for an explanation of the increasing “repulsivity” from ² $\Pi(\tilde{X}^2\Pi)$ to ² Δ to ² Σ^+ we refer to Ref. 1.

Although according to our calculations the first bound state of ScN₂ seems to be of bent geometry (⁴ B_1), for reasons of convenience and clarity we begin the discussion from the lowest linear state of ⁴ Σ^- symmetry, about 2 kcal/mol above the ⁴ B_1 at the RCCSD(T)/ANO+AQZ level of theory, see Fig. 1 and Table II. Disregarding the repulsive ² $\Pi, ^2\Delta$, and ² Σ^+ states which correlate to $\text{Sc}(^2D)$, the next five bound states are, arbitrarily tagged, $1^4B_1, 2^4\Sigma^-, 3^4B_2, 4^4A_2$, and $5^4\Phi$.

The bonding of the $2^4\Sigma^-$ state of ScN₂ is represented graphically by the vbL diagram (1), indicating a σ -dative charge transfer from N₂ to the Sc empty hybrid orbital, while the $4s$ electron of the free Sc at equilibrium is distributed in the opposite side of the incoming ligand occupying now a $\sim 4s3d_{\sigma}4p_z$ metal hybrid. In addition, the bonding is significantly assisted due to the $(3d\pi_x, 3d\pi_y) - (2p\pi_x, 2p\pi_y)$ conjugation. Because of the rather weak interactions of all states in the MN_2 systems, the wave function at equilibrium can be described adequately by the antisymmetrized product of the two fragment wave functions at infinity, namely, $\Psi(MN_2) = \hat{A}\Psi(M) * \Psi(N_2)$, where $\Psi(N_2) = |1\sigma_g^2 1\sigma_u^2 2\sigma_g^2 1\pi_u^4\rangle$, counting only the valence electrons of N₂. Indeed, suppressing the 18 core electrons of Sc, the leading equilibrium MRCI configurations of the ScN₂ $2^4\Sigma^-$ state, are

$$\begin{aligned}
 |2^4\Sigma^-\rangle &\simeq |1\sigma^2 2\sigma^2 3\sigma^2 1\pi^4 [(0.91)4\sigma^1 2\pi_x^1 2\pi_y^1 \\
 &\quad + (0.24)4\sigma^1 1\delta_+^1 1\delta_-^1]\rangle \\
 &\simeq \hat{A}\Psi(N_2) * \Psi(\text{Sc}, ^4F; M_L = 0).
 \end{aligned}$$

Observe that the coefficients 0.91 and 0.24 are very close to the $(4/5)^{1/2} = 0.89$, $(1/5)^{1/2} = 0.45$ atomic coefficients entering in the $^4F(M_L=0)$ description of Sc, $|^4F; M_L=0\rangle = \sqrt{4/5}|4s^1 3d\pi_x^1 3d\pi_y^1\rangle + \sqrt{1/5}|4s^1 3d_{\delta+}^1 3d_{\delta-}^1\rangle$. The MRCI Mulliken atomic equilibrium populations (Sc/N/N)

TABLE II. Total energies $E(E_h)$, equilibrium bond distances r_e (Å), dissociation energies D_e/D_0 (kcal/mol), harmonic frequencies ω_i (cm^{-1}), dipole moments μ (D), and energy separations T_e (cm^{-1}) of $M\text{N}_2$ species, $M=\text{Sc, Ti, V, and Cr}$.

Method	$-E$	D_e/D_0	$r_{M-\text{NN}}^a$	$r_{M\text{N}-\text{N}}$	T_e	$\omega_1,^b \omega_2, \omega_3$	$\langle\mu\rangle/\mu_{\text{FF}}^c$
ScN₂							
1 ⁴B₁							
MRCI ^d	869.138 75	16.6	2.223(2.147)	1.157	0.0		-1.99/-2.10
MRCI+Q ^d	869.191 16	18.7	2.217(2.139)	1.167	0.0		/-2.05
RCCSD(T) ^e	869.163 40	23.2/22.8	2.256(2.178)	1.179	0.0	388, 401, 1830	/-2.19
C-RCCSD(T) ^e	869.461 84	26.0	2.181(2.101)	1.174	0.0		/-2.19
C-RCCSD(T)+DKH2 ^e	873.112 16	23.6	2.183(2.102)	1.175	0.0		
2 ⁴Σ⁻							
MRCI ^d	869.122 00	9.77	2.089	1.111	3676		-0.40/-1.42
MRCI+Q ^d	869.182 58	16.6	2.030	1.136	1884		/-3.61
RCCSD(T) ^e	869.160 51	21.4/20.4	2.045	1.158	635	280, 429, 2028	/-3.78
RCCSD(T)+DKH2 ^e	872.764 74	23.1	2.041	1.157			/-3.63
C-RCCSD(T) ^e	869.459 73	24.7	2.014	1.147	463		/-3.25
C-RCCSD(T)+DKH2 ^e	873.108 87	21.5	2.017	1.148	722		/-3.53
RCCSD(T) ^f	869.169 60	21.5	2.043	1.157			/-3.61
RCCSD(T)+DKH2 ^f	872.772 59	23.1	2.042	1.155			/-3.65
C-RCCSD(T) ^g	869.530 01	20.8	2.024	1.144			/-3.10
C-RCCSD(T)+DKH2 ^g	873.132 84	22.0	2.019	1.146			/-3.27
3 ⁴B₂							
MRCI ^d	869.136 14	14.9	2.251(2.175)	1.155	573		-2.01/-2.07
MRCI+Q ^d	869.188 00	16.8	2.252(2.175)	1.165	694		/-2.01
RCCSD(T) ^e	869.159 53	20.8	2.298(2.221)	1.176	850		/-2.17
4 ⁴A₂							
MRCI ^d	869.128 78	10.3	2.273(2.199)	1.150	2189		-1.90/-1.82
MRCI+Q ^d	869.181 12	12.4	2.274(2.199)	1.160	2205		/-1.68
RCCSD(T) ^e	869.153 35	16.9	2.322(2.247)	1.178	2206		
5 ⁴Φ							
MRCI ^d	869.126 40	9.14	2.127	1.129	2711		-3.53/-3.25
MRCI+Q ^d	869.178 67	11.1	2.127	1.137	2741		/-3.15
RCCSD(T) ^e	869.152 53	16.4	2.147	1.147	2386		/-3.33
TiN₂							
1 ⁵Δ							
MRCI ^d	957.779 63	2.80	2.204	1.090	0.0		+2.08/+1.32
MRCI+Q ^d	957.831 14	6.79	2.054	1.115	0.0		/-0.36
RCCSD(T) ^e	957.860 07	13.8/13.1	2.010	1.134	0.0	271, 384, 1938	/-2.10
RCCSD(T)+DKH2 ^e	962.251 82	15.3	2.010 ^h	1.134 ^h	0.0		/-2.17
C-RCCSD(T) ^e	958.187 44	16.6	1.992	1.130	0.0		/-1.85
C-RCCSD(T)+DKH2 ^e	962.627 16	14.3	1.990	1.132	0.0		/-1.98
RCCSD(T) ^f	957.869 62	14.0	2.008	1.134	0.0		/-2.05
RCCSD(T)+DKH2 ^f	962.260 06	15.4	2.008	1.134	0.0		/-2.18
C-RCCSD(T) ^g	958.262 50	12.5	2.001	1.131	0.0		/-1.98
C-RCCSD(T)+DKH2 ^g	962.652 52	13.8	2.001 ^h	1.131 ^h	0.0		/-1.80
2 ⁵A₁							
MRCI ^d	957.774 51	0.65	2.212(2.137)	1.141	1126		-1.18/-1.14
MRCI+Q ^d	957.826 26	4.3	2.218(2.143)	1.147	1070		/-0.99
RCCSD(T) ^e	957.851 53	8.45/8.09	2.207(2.129)	1.159	1875	346, 381, 1837	/-1.40
C-RCCSD(T) ^e	958.176 71	9.87	2.175(2.097)	1.155	2354		/-1.20
C-RCCSD(T)+DKH ^e	962.617 22	8.1	2.175(2.097)	1.155	2182		
3 ⁵A₂							
MRCI ^d	957.776 93	1.60	2.229(2.154)	1.145	595		-1.24/-1.55
MRCI+Q ^d	957.826 59	4.5	2.242(2.167)	1.150	998		/-1.27
RCCSD(T) ^e	957.849 69	7.30	2.234(2.157)	1.159	2278		/-1.57
4 ⁵B₁							
MRCI ^d	957.770 49	-2.4	2.231(2.156)	1.146	2006		-0.71
MRCI+Q ^d	957.820 77	0.81	2.240(2.165)	1.151	2277		/-0.18

TABLE II. (Continued.)

Method	$-E$	D_e/D_0	r_{M-NN}^a	r_{MN-N}	T_e	$\omega_1,^b \omega_2, \omega_3$	$\langle\mu\rangle/\mu_{FF}^c$
RCCSD(T) ^e	957.843 68	3.52	2.228(2.151)	1.160	3598		
MRCI+Q ^d	957.814056	13.2	2.021	1.121	3749		/-0.65
VN₂							
1⁶Σ⁺							
MRCI ^d	1052.294 43	0.67	2.316	1.084	0.0		+2.75/+2.41
MRCI+Q ^d	1052.347 25	2.75	2.186	1.098	0.0		
RCCSD(T) ^e	1052.374 19	6.96/6.12	2.027	1.115	0.0	276, 279, 2131	/-0.29
RCCSD(T)+DKH ^e	1057.678 93	7.87	2.027 ^h	1.115 ^h	0.0		/-0.35
C-RCCSD(T) ^e	1052.723 18	10.2	2.006	1.114	0.0		/-0.21
C-RCCSD(T)+DKH2 ^e	1058.077 55	8.03	2.002	1.115	0.0		/-0.36
RCCSD(T) ^f	1052.384 56	6.99	2.022	1.114	0.0		/-0.25
RCCSD(T)+DKH2 ^f	1057.687 84	7.92	2.022	1.114	0.0		/-0.38
C-RCCSD(T) ^g	1052.804 82	6.98	2.024	1.112	0.0		/-0.23
C-RCCSD(T)+DKH2 ^g	1058.107 92	7.76	2.024 ^h	1.112 ^h	0.0		/-0.21
2⁶A₁							
RCCSD(T) ^e	1052.362 66	-0.27	2.165(2.088)	1.146	2530		
C-RCCSD(T) ^e	1052.709 34	1.47	2.144(2.066)	1.145	3039		
3⁶Δ							
RCCSD(T) ^e	1052.361 67	-0.89	2.205	1.108	2747		
C-RCCSD(T) ^e	1052.709 11	1.33	2.194	1.107	3088		
CrN₂							
5⁵Σ⁺							
MRCI+Q ^d	1152.817 04	0.51	2.164	1.093			/+2.76
7⁷Π							
MRCI ^d	1152.717 31	13.9	1.959	1.123			-2.89/-2.62
MRCI+Q ^d	1152.771 09	17.1	1.898	1.152	10 085		/-5.40
RCCSD(T) ^e	1152.810 72	27.0	1.974	1.138			/-4.11
7⁷B₂							
MRCI ^d	1152.727 39	19.6	2.216(2.140)	1.156			
MRCI+Q ^d	1152.783 61	22.3	2.200(2.122)	1.166	7336		
RCCSD(T) ^e	1152.808 22	25.4	2.205(2.125)	1.175			
7⁷B₁							
RCCSD(T) ^e	1152.772 11	2.79	2.584(2.524)	1.104			

^aValues in parenthesis refer to $M-N_2$ distances from the middle of the $-N\equiv N-$ bond.

^bDoubly degenerate for linear species.

^c $\langle\mu\rangle$ calculated as expectation value; μ_{FF} calculated by the finite field approach. In all cases the metal is at the origin of the coordinate system, with the N₂ molecule along the z axis in the linear species. This means that negative dipole moments correspond to the polarity $M^+-N_2^-$.

^dANO+QZ basis set, see text.

^eANO+AQZ basis set, see text.

^f5Z basis set, see text.

^gC5Z basis set, see text.

^hGeometry at the C-RCCSD(T)/C5Z level.

$$4s^{0.85}4p_z^{0.19}3d_{z^2}^{0.11}3d_{xz}^{0.81}3d_{yz}^{0.81}/_{Sc}2s^{1.58}2p_z^{1.24}2p_x^{1.08}2p_y^{1.08} \\ \times 3d^{0.10}/_N2s^{1.73}2p_z^{1.19}2p_x^{1.01}2p_y^{1.01}3d^{0.10}/_N$$

indicate a weak flow of electrons from Sc to N₂, or to be more specific $Sc^{+0.16}-N^{-0.11}-N^{-0.05}$. Around $0.15e^-$ is transferred via the σ -frame from N₂ to Sc, while about $0.30e^-$ is fed back to N₂ through the π system. Certainly, the central nitrogen feels mainly the bonding perturbation with the terminal one remaining practically intact. This can be seen by contrasting the $-NN$ populations above with the distribu-

tions of the free N₂ at the same level of theory: $2s^{1.74}2p_z^{1.22}2p_x^{0.97}2p_y^{0.97}3d^{0.10}$ Diagram (1) clearly captures the bonding character which is identical to that of the ScCO $\tilde{X}^4\Sigma^-$ state.¹ Even the magnitudes of dipole moments of the $4\Sigma^-$ states of ScN₂ and ScCO are very similar, 3.78 and 3.34 D, respectively, at the RCCSD(T)/ANO+AQZ level (see also footnote c of Table II as to the sign of dipole moment).

Let us examine now in some detail the binding energy D_e of the ScN₂ $2^4\Sigma^-$ state as a function of the method/basis set used, see Table II. The inadequacy of the size-nonextensive MRCI method is obvious: $D_e=9.8$ kcal/mol

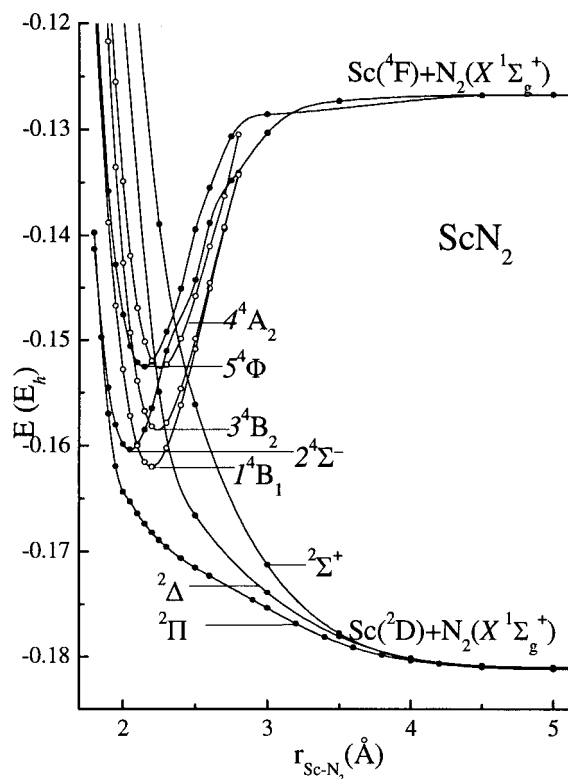


FIG. 1. RCCSD(T)/ANO+AQZ potential energy profiles (PEPs) of Sc-N₂. All energies shifted by +869.0 E_h.

which becomes 16.6 kcal/mol by adding the Davidson correction. At the RCCSD(T)/ANO+AQZ level the D_e jumps to 21.4 kcal/mol, increasing further to 23.1 kcal/mol by taking into account scalar relativity, RCCSD(T)+DKH2/ANO+AQZ. By including core excitations, but with no extra

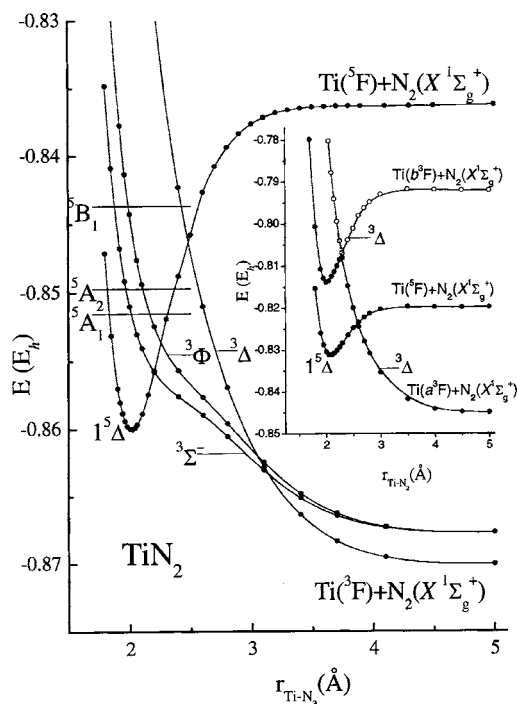


FIG. 2. RCCSD(T)/ANO+AQZ PEPs of Ti-N₂ and $1^5\Delta$, 3Δ PEPs at the MRCI+Q/ANO+QZ level (inset). All energies shifted by +957.0 E_h.

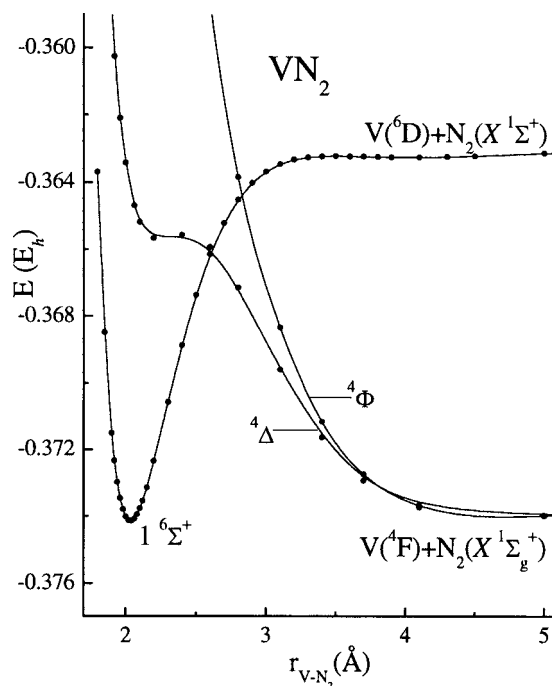


FIG. 3. RCCSD(T)/ANO+AQZ PEPs of V-N₂. All energies shifted by +1052.0 E_h.

functions in the basis sets, [C-RCCSD(T)/ANO+AQZ], the D_e becomes 24.7 kcal/mol, an increase of 24.7-21.4 = 3.3 kcal/mol. Including at this level the DKH2 effects [C-RCCSD(T)+DKH/ANO+AQZ] D_e decreases by 3.2 kcal/mol, returning to the RCCSD(T)/ANO+AQZ result, $D_e=21.5$ kcal/mol. Defining differences (δ) between D_e values according to the methodology used in an obvious notation, namely, $\delta_{\text{rel}} \equiv D_e[\text{RCCSD(T)+DKH2}] - D_e[\text{RCCSD(T)}]$, $\delta_C \equiv D_e[\text{C-RCCSD(T)}] - D_e[\text{RCCSD(T)}]$, and $\delta_{C+\text{rel}} \equiv D_e[\text{C-RCCSD(T)+DKH2}] - D_e[\text{RCCSD(T)}]$, the previous discussion can be epitomized as follows (all numbers in kcal/mol):

$$\delta_{\text{rel}}^B = 23.1 - 21.4 = 1.7, \quad \delta_C^B = 24.7 - 21.4 = 3.3,$$

$$\text{and } \delta_{C+\text{rel}}^P = 21.5 - 21.4 = 0.1.$$

The superscript B refers to the ANO basis set of Bauschlicher. The corresponding δ values using the Peterson basis set (δ^P) are (Table II)

$$\delta_{\text{rel}}^P = 23.1 - 21.5 = 1.6, \quad \delta_C^P = 20.8 - 21.5 = -0.7,$$

$$\text{and } \delta_{C+\text{rel}}^B = 22.0 - 21.5 = 0.5.$$

We conclude that (a) D_e values are practically identical in both basis sets when excitations are limited within the valence space. This is quite interesting if one thinks that the P (5Z) basis is almost twice as large (153 functions on M) as compared to the B (ANO) basis set (84 functions on M). This holds true with (+DKH2) or without scalar relativistic corrections. (b) Including core excitations, however, an opposite effect is observed between the two basis sets: the B set increases the D_e value by 3.3 kcal/mol, while the P set decreases the D_e by 0.7 kcal/mol. (c) Including now the relativistic effects to the core wave functions, again an opposite effect is observed: The B set decreases the D_e value by

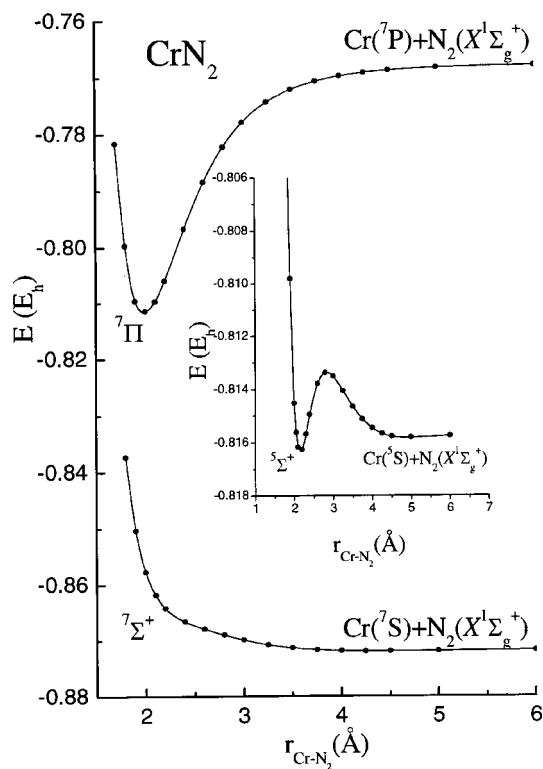


FIG. 4. RCCSD(T)/ANO+AQZ PEPs of Cr-N₂, and $5\Sigma^+$ PEP at the MRCI+Q/ANO+QZ level (inset). All energies shifted by +1152.0 E_h .

3.2 kcal/mol, while the P set increases the D_e by 1.2 kcal/mol, see Table II. (d) Notice that $\delta_{C+rel}^P = 0.5$ kcal/mol $\approx \delta_{rel}^P + \delta_C^P$ ($=0.9$ kcal/mol), an intuitively appealing result. This does not hold for the B basis set, where $\delta_{C+rel}^B = 0.1$ kcal/mol, but $\delta_{rel}^B + \delta_C^B = 1.7 + 3.3 = 5.0$ ($\neq 0.1$) kcal/mol. Remarkably, both basis sets end up to almost the same binding energy at the C-RCCSD(T)+DKH2 level (21.5 vs 22.0 kcal/mol), in essence identical to the simple RCCSD(T) D_e value (21.4 vs 21.5 kcal/mol), an interesting case of the “right result for the wrong reason” in the case of the B basis set when core excitations are included, but with no appropriately optimized core functions. The conclusions above are shown graphically in Fig. 5. At the highest level of theory C-RCCSD(T)+DKH2/C5Z, $D_e(D_0) = 22.0(21.0)$ kcal/mol at $r_{Sc-NN} = 2.024$ Å. The zero point energy (ZPE) correction refers to the harmonic frequencies obtained at the RCCSD(T)/ANO+cc-pVTZ level. It should be mentioned here that at the DFT(B3LYP) level, the D_e of $4\Sigma^-$ is 35.0 kcal/mol.⁵

Among the quartets, the lowest state belongs to B_1 symmetry (C_{2v}), 635 (463) [722] cm^{-1} below the $4\Sigma^-$ state at the RCCSD(T) (C-RCCSD(T)) [C-RCCSD(T)+DKH2]/ANO+AQZ level of theory (Table II and Fig. 1). The atomic MRCI Mulliken populations at infinity [$Sc(4F) + N_2(X^1\Sigma_g^+); r_\infty$] and equilibrium ($1^4B_1; r_e$) are

$$r_\infty: 4s^{1.0} 4p_z^{0.0} 3d_{z^2}^{0.14} 3d_{xz}^{0.18} 3d_{yz}^{0.83} 3d_{xy}^{0.82} / Sc 2s^{1.75} 2p_z^{0.96} 2p_x^{0.96} \times 2p_y^{1.21} / N,$$

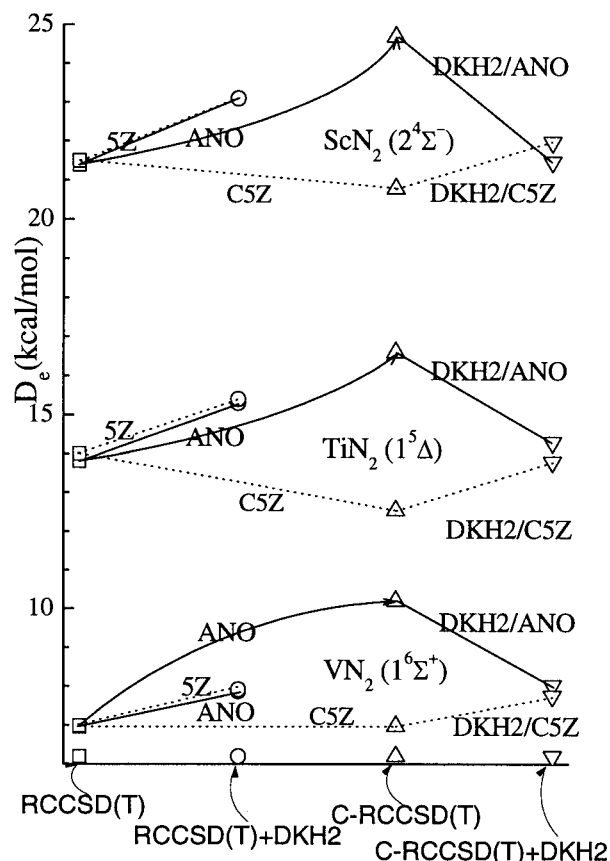


FIG. 5. Dissociation energies (D_e) of $ScN_2(2^4\Sigma^-)$, $TiN_2(1^5\Delta)$, and $VN_2(1^6\Sigma^+)$ in relation to method/basis set. Solid lines are ANO basis sets, and dotted lines are 5Z and C5Z basis sets. See text.

$$r_e: 4s^{0.83} 4p_z^{0.30} 3d_{z^2}^{0.09} 3d_{xz}^{0.04} 4p_x^{0.02} 3d_{yz}^{0.20} 4p_y^{0.05} 3d_{xy}^{0.99} / Sc 2s^{1.72} \times 2p_z^{1.30} 2p_x^{0.94} 2p_y^{1.14} / N.$$

The leading MRCI equilibrium configuration is $|1^4B_1\rangle \approx 0.94|1a_1^2 2a_1^2 3a_1^2 4a_1^2| 1b_1^2 1b_2^2 2b_1^2 1a_2^2\rangle$ counting the 13 valence electrons. The explicit forms of the MRCI equilibrium orbitals are of importance in order to understand the bonding in the 1^4B_1 state.

$$1a_1 \approx (0.88)2s^N - (0.17)2p_y^N, \quad 2a_1 \approx 2p_y^N,$$

$$3a_1 \approx 2p_z^N, \quad 4a_1 \approx (0.71)4s^{Sc} + (0.45)4p_z^{Sc},$$

$$1b_1 \approx (0.87)2p_x^N, \quad 1b_2 \approx (0.91)2s^N + (0.40)2p_y^N,$$

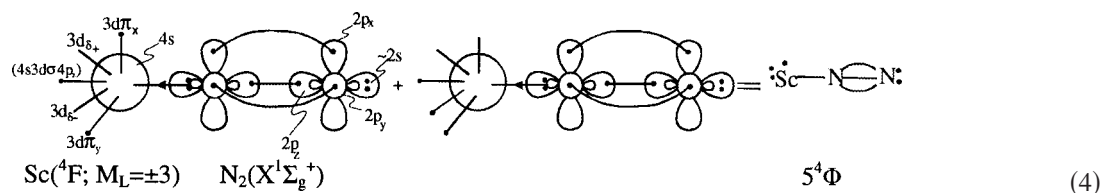
$$2b_2 \approx (0.89)2p_z^N - (0.33)3d_{yz}^{Sc}, \quad 1a_2 \approx (0.99)3d_{xy}^{Sc}.$$

According to the Mulliken densities, the bonding is caused by the transfer of about $0.6e^-$ from the $3d_{yz}$ orbital of Sc to the “antibonding” $2\pi p_z$ space of N₂ realized by the $2b_2$ orbital. The interaction is shown graphically by the vBL diagram (2). In a different language, the Sc-N₂ charge transfer can be thought as a $2p_z^N - 3d_{yz}^{Sc}$ “conjugation” with a synchronous weakening of the $2\pi p_z$ (N₂) bond. This is reflected to the considerable N-N bond lengthening and decrease of the corresponding harmonic frequency in the 1^4B_1 state, as com-

pared to the free N₂ at the same level ($r_e=1.1005 \text{ \AA}$, $\omega_e=2346 \text{ cm}^{-1}$), see Table II. In total, $0.42e^-$ migrate from the metal to the N₂ moiety.

Comparing our numbers of the $2^4\Sigma^-$ and 1^4B_1 states of ScN₂ with the DFT (BP86) results of Ref. 4, we observe similar geometries but a reversal of ordering of the two states, i.e., the 4B_1 is above the $^4\Sigma^-$ by 2.5 kcal/mol. Also, the N–N stretching frequencies (ω_3) are predicted 86 (4B_1) and 158 ($^4\Sigma^-$) cm^{-1} smaller than the present results (Table II).

The next two ScN₂ states are of bent symmetry (C_{2v}), 850 (3^4B_2) and 2206 (4^4A_2) cm^{-1} above the 1^4B_1 at the RCCSD(T) level. Note, however, the ordering reversal between the 3^4B_2 and $2^4\Sigma^-$ states at the MRCI+Q approach (Table II). Trusting more our coupled-cluster results the binding energies are calculated to be 20.8 and 16.9 kcal/mol with respect to Sc(4F)+N₂($X^1\Sigma_g^+$) for the 3^4B_2 and 4^4A_2 states, respectively. In all three T-shaped states the bonding has the same character, with the “spectator” electron moving from the $3d_{xy}$ (1^4B_1) to $3d_{x^2-y^2}$ (3^4B_2) to $3d_{xz}$ (4^4A_2). This is



Contrasting diagram (4) with (1) we infer that the Sc–N–N(Sc–NN) bond length(s) should decrease (increase) as compared to the $2^4\Sigma^-$ state, accompanied of course by a significant loss in the Sc–N₂ bond strength. Indeed, at the RCCSD(T)/ANO+AQZ level the Sc–N–N bond distance decreases by 0.011 Å , the Sc–NN increases by 0.102 Å , whereas the Sc–NN dissociation energy is losing 5.0 kcal/mol as compared to the corresponding values of the $2^4\Sigma^-$ state.

B. TiN₂

In the presence of N₂ in an axial geometry the ground $^3F(4s^23d^2)$ state of Ti atom gives rise to four molecular states of $^3\Sigma^-$, $^3\Pi$, $^3\Delta$, and $^3\Phi$ symmetries. As previously discussed (see also Ref. 1) all these triplets are expected to be repulsive, and indeed they are as shown in Fig. 2 (but see below). Although $^3\Pi$ symmetry is not shown because it is not accessible via the coupled-cluster method, it is also repulsive as confirmed by MRCI calculations. Corresponding bent triplets should also be of repulsive character.

Now, the lowest linear state correlating to the first excited state of Ti($^5F; 4s^13d^3$)+N₂($X^1\Sigma_g^+$) is of $^5\Delta$ symmetry. The bonding is similar to that of $1^4\Sigma^-$ state of ScN₂, there-

also clear from the equilibrium MRCI populations which are practically the same in all three C_{2v} states, the only difference being the occupation of $3d_{xy}$, $3d_{x^2-y^2}$, or $3d_{xz}$ orbitals,

$$3^4B_2: 4s^{0.84}4p_z^{0.30}3d_{z^2}^{0.09}3d_{xz}^{0.04}4p_x^{0.02}3d_{yz}^{0.20}4p_y^{0.05} \\ \times 3d_{x^2-y^2}^{0.99}/_{Sc}2s^{1.72}2p_z^{1.30}2p_x^{0.93}2p_y^{1.14}/_N, \\ 4^4A_2: 4s^{0.86}4p_z^{0.27}3d_{z^2}^{0.08}3d_{xz}^{0.99}4p_x^{0.04}3d_{yz}^{0.21}4p_y^{0.06}/_{Sc}2s^{1.72} \\ \times 2p_z^{1.29}2p_x^{0.94}2p_y^{1.14}/_N.$$

Certainly, the same net charge transfer is observed from Sc to N₂ in these three states amounting to about $0.4e^-$, whereas consistently enough dipole moments are close to 2 D. Finally, the N–N bond length does not vary by more than 0.003 Å as we move from 1^4B_1 to 3^4B_2 to 4^4A_2 .

The last calculated ScN₂ state is of $^4\Phi$ symmetry, degenerate with the 4^4A_2 one at the RCCSD(T)/ANO+AQZ level and completely analogous to the $\tilde{A}^4\Phi$ state of ScCO (Ref. 1), see diagram (4).

fore described by the vbl diagram (1) with an additional (spectator) electron to a δ_{\pm} atomic orbital of Ti. The MRCI equilibrium atomic populations (Ti/N/N)

$$4s^{0.89}4p_z^{0.17}3d_{z^2}^{0.07}3d_{xz}^{0.94}3d_{yz}^{0.94}3d_{x^2-y^2}/_{Ti}2s^{1.60}2p_z^{1.24}2p_x^{1.02} \\ \times 2p_y^{1.02}3d^{0.11}/_N2s^{1.72}2p_z^{1.20}2p_x^{0.96}2p_y^{0.96}3d^{0.10}/_N$$

are very similar to those of the ScN₂ $1^4\Sigma^-$ state, but with a slightly smaller, albeit noticeable, charge transfer from Ti to –N₂ through the double π route. *Mutatis mutandis* the bonding mechanism is identical to the $1^4\Sigma^-$ state of ScN₂, but with a binding energy smaller by about 8 kcal/mol, see Table II. Using the δ notation introduced earlier in relation to the D_e values according to different methodologies, we can write (all numbers in kcal/mol)

$$\delta_{rel}^B = 15.3 - 13.8 = 1.5, \quad \delta_C^B = 16.6 - 13.8 = 2.8,$$

$$\delta_{C+rel}^B = 14.3 - 13.8 = 0.5 (\neq 1.5 + 2.8),$$

$$\delta_{rel}^P = 15.4 - 14.0 = 1.4, \quad \delta_C^P = 12.5 - 14.0 = -1.5,$$

$$\delta_{C+rel}^P = 13.8 - 14.0 = -0.2 (\approx 1.4 - 1.5).$$

In every respect our conclusions are consistent with those in connection with the $1^4\Sigma^-$ state of ScN₂ (*vide supra*). Figure 5 shows graphically our δ analysis. At the highest

level of calculation C-RCCSD(T)+DKH2/C5Z, $D_e(D_0) = 13.8(13.1)$ kcal/mol with respect to $\text{Ti}(^5F) + \text{N}_2(X^1\Sigma_g^+)$ at $r_{\text{Ti-N}} = 2.001$ Å. Concerning the magnitude of dipole moment of the $1^5\Delta$ state of TiN_2 we can recommend a value of 2 D, but notice the preposterous results obtained at the MRCI or MRCI+Q level of theory (Table II). The DFT(B3LYP) D_e value of Pilme *et al.*⁵ is 30 kcal/mol, more than twice as large than the present value.

We return now to the $^3\Delta$ state, clearly repulsive at the CC method. However, as the inset of Fig. 2 indicates, this state is bound at the MRCI(+Q) level due to an avoided crossing with an incoming state correlating to $\text{Ti}(b^3F; 4s^1 3d^3) + \text{N}_2(X^1\Sigma_g^+)$, a situation completely analogous to the $\text{TiCO } \tilde{a}^3\Delta$ state (Ref. 1). For reasons of comparison the PEP of $1^5\Delta$ state is also shown in Fig. 2. Although we cannot locate accurately enough the relative position of the $^3\Delta$ state because it is inaccessible at the RCCSD(T) single reference method, at the MRCI+Q level it displays a binding energy of 13.2 kcal/mol. “Scaling” this value with respect to the binding energy of the $1^5\Delta$ state at the RCCSD(T)/ANO+AQZ and MRCI+Q/ANO+QZ, i.e., $13.8 - 6.8 = 7$ kcal/mol, we can claim that $D_e(^3\Delta) \approx 20$ kcal/mol with respect to $\text{Ti}(b^3F) + \text{N}_2(X^1\Sigma_g^+)$ fragments.

Three bent states of C_{2v} symmetry have been examined at the RCCSD(T) and MRCI+Q level, namely, 2^5A_1 , 3^5A_2 , and 4^5B_1 , all correlating to the first excited state of $\text{Ti}(^5F)$, with RCCSD(T) (MRCI+Q) binding energies of $D_e = 8.5$ (4.3), 7.3 (4.5), and 3.5 (0.81) kcal/mol, respectively. Their RCCSD(T) location is indicated in Fig. 2 by horizontal lines. Because the equilibrium MRCI populations of, say, the 2^5A_1 state are identical to those of the 4^5B_1 state of ScN_2 [+ a spectator $3d_{xz}(b_1)$ electron], for the bonding interaction of these bent states we refer to the vbL diagram (2) and the relevant discussion.

C. VN₂

Interacting linearly with $\text{N}_2(X^1\Sigma_g^+)$ the ground state of $\text{V}(^4F; 4s^2 3d^3)$ gives rise to $^4\Sigma^+$, $^4\Pi$, $^4\Delta$, and $^4\Phi$ molecular states. The PEPs of $^4\Delta$ and $^4\Phi$ are shown in Fig. 3 and they are repulsive as expected. The $^4\Sigma^+$ and $^4\Pi$ states are not accessible via the CC method, however, both should also be of repulsive character.

From the first excited state of $\text{V}(^6D; 4s^1 3d^4)$ [experimentally⁶ (calculated) 0.245 (0.297–0.258) eV higher] three (linear) sextets are obtained, namely, $^6\Sigma^+$, $^6\Pi$, and $^6\Delta$. Figure 3 displays the RCCSD(T)/ANO+AQZ $^6\Sigma^+$ PEP, the only bound state among the sextets. The $^6\Delta$ state is either repulsive or slightly attractive (Table II), and although the $^6\Pi$ has not been calculated, its behavior should be similar to the $^6\Delta$ state.

At the highest level of theory, C-RCCSD(T)+DKH2/C5Z, the $^6\Sigma^+$ state is bound by 7.76 kcal/mol with respect to the adiabatic fragments, or $D_0 = 6.92$ kcal/mol after the ZPE correction [the DFT(B3LYP) D_e value is three times higher⁵]. It is interesting to follow the δ analysis of D_e which shows a similar pattern as in the ScN_2 and TiN_2 cases (all numbers in kcal/mol),

$$\delta_{\text{rel}}^B = 7.87 - 6.96 = 0.91, \quad \delta_C^B = 10.2 - 6.96 = 3.24,$$

$$\delta_{C+\text{rel}}^B = 8.03 - 6.96 = 1.07 (\neq 0.91 + 3.24),$$

$$\delta_{\text{rel}}^P = 7.92 - 6.99 = 0.93, \quad \delta_C^P = 6.98 - 7.92 = -0.94,$$

$$\delta_{C+\text{rel}}^P = 7.76 - 7.92 = -0.16 (\approx 0.93 - 0.94).$$

The above is shown diagrammatically in Fig. 5. The binding interaction of the ground state sextet $1^6\Sigma^+$ is shown graphically in diagram (1) by adding two δ_{\pm} electrons in the $^4\Sigma^-$ state of ScN_2 .

D. CrN₂

The linear approach of N_2 to the ground state of $\text{Cr}(^7S)$ gives rise to a single molecular state of $^7\Sigma^+$ symmetry, obviously of repulsive character, see Fig. 4. The corresponding bent structure of CrN_2 ($C_s; ^7A'$) is of repulsive nature as well. This is in stark contrast with the findings of Pilme *et al.*⁵; these workers obtained a binding energy of 13.3 kcal/mol for the $^7A'$ state of CrN_2 with respect to $\text{Cr}(^7S) + \text{N}_2(X^1\Sigma_g^+)$ at the DFT (B3LYP) level.

The next state stems from the $^5S(4s^1 3d^5)$ term of Cr, differing by a single spin flip from the 7S term, experimentally 0.941 eV above the 7S state.⁶ At the MRCI(+Q)/ANO level the $^5S \leftarrow ^7S$ splitting is calculated to be 0.855 (0.851) eV. The related molecular $^5\Sigma^+$ CrN_2 state, inaccessible at the CC approach, is MRCI unbound but van der Waals attractive (~ 0.5 kcal/mol) with respect to the adiabatic atoms (Fig. 4) after adding the Davidson correction.

It is interesting to examine what is the next Cr atomic state which could give rise to a substantially attractive interaction with the N_2 molecule. According to the Moore tables⁶ the second excited state of Cr located 1.003 eV higher, just 0.062 eV above the 5S term, is of $^5D(4s^2 3d^4)$ symmetry, not a promising candidate for a relatively strong CrN_2 bound quintet (*vide supra*). Within a 0.610 eV range a bundle of nine states follow, namely, $^5G(4s^1 3d^5)$, $^5P(4s^1 3d^5)$, $^3P(4s^2 3d^4)$, $^7P(4p^1 3d^5)$, $^3H(4s^2 3d^4)$, $^5D(4s^1 3d^5)$, $^3G(4s^1 3d^5)$, $^3F(4s^2 3d^4)$, and $^7F(4s^1 4p^1 3d^4)$ with M_j averaged splittings of 2.541, 2.709, 2.950, 2.903, 2.985, 3.012, 3.092, 3.117, and 3.153 eV, respectively. The CrN_2 states emerging from the Cr terms with configuration $4s^2 3d^4$ (3P , 3H , and 3F) are certainly repulsive (see Sec. I). The molecular states correlating to $4s^1 3d^5$ (5G , 5P , 5D , and 3G) should be of repulsive character as well due to the presence of a $3d\sigma$ (singly) occupied orbital and in agreement with our results on the $^7\Sigma^+$ and $^5\Sigma^+$ states of CrN_2 . Therefore, only the $^7P(4p^1 3d^5)$ state is worth of examining, but as we will see the $^7F(4s^1 4p^1 3d^4)$, 0.250 eV above the 7P , is also entangled in the bonding.

The 7P gives rise to a $^7\Pi$ CrN_2 state under linear attack. However, the equilibrium Mulliken MRCI densities (r_e) and the corresponding ones at infinity (r_∞),

$$\begin{aligned} r_e: & 4s^{0.80} 4p_z^{0.15} 3d_{z^2}^{0.28} 4p_x^{0.44} 3d_{xz}^{1.0} 3d_{yz}^{1.0} 3d_{x^2-y^2}^{1.0} 3d_{xy}^{1.0} / \text{Cr} \\ & \times 2s^{1.53} 2p_z^{1.24} 2p_x^{1.30} 2p_y^{1.07} 3d^{0.10} / \text{N} 2s^{1.69} 2p_z^{1.21} 2p_x^{1.19} \\ & \times 2p_y^{0.86} 3d^{0.1} / \text{N}, \end{aligned}$$

TABLE III. Total energies E (E_h), dissociation energies D_e/D_0 (kcal/mol), geometries r_e (Å), and harmonic frequencies ω_e (cm^{-1}) of the linear tetraatomics ScN_2Sc (${}^7\Sigma_u^+$), TiN_2Ti (${}^9\Gamma_g$), VN_2V (${}^{11}\Sigma_u^+$), and CrN_2Cr (${}^{13}\Sigma_g^-$ and ${}^{13}\Delta_g$) in different methodologies.

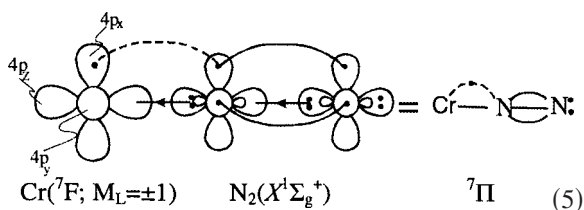
Method	$-E$	D_e/D_0^a	r_{M-NN}	r_{MN-NM}	$\omega_{-N\equiv N}^b$
Sc—N ₂ —Sc					
RCCSD(T)	1628.925 05	49.9	2.048	1.235	
C-RCCSD(T)	1629.513 77	50.4	2.030	1.194	
C-RCCSD(T)+DKH2	1636.751 39	43.5	2.024	1.200	
Ti—N ₂ —Ti					
RCCSD(T)	1806.314 12	28.4/27.4	2.045	1.161	1705
C-RCCSD(T)	1806.969 62	34.4	2.035	1.149	
C-RCCSD(T)+DKH2	1815.787 27	28.5	2.036	1.151	
V—N ₂ —V					
RCCSD(T)	1995.343 62	15.5/14.3	2.032	1.130	1984
C-RCCSD(T)	1996.042 55	22.5	2.013	1.128	
C-RCCSD(T)+DKH2	2006.690 07	17.3	2.017	1.129	
Cr—N ₂ —Cr					
RCCSD(T) (${}^{13}\Sigma_g^-$)	2196.217 31	56.0	2.034	1.157	
RCCSD(T) (${}^{13}\Delta_g$)	2196.216 02	55.2	2.021	1.148	

^a $D_0 = D_e - \text{ZPE} = D_e - \sum_i \frac{1}{2} \omega_i (MN_2M) + \frac{1}{2} \omega_e (N_2)$.

^bHarmonic stretching frequencies of $-N\equiv N-$. The remaining six harmonic frequencies for TiN_2Ti and VN_2V are 61, 61, 233, 292, 292, 402 cm^{-1} , and 71, 71, 194, 264, 301, 301 cm^{-1} , respectively. The calculation of the harmonic frequencies $\{\omega_i\}$ was done using a smaller basis set ANO-g+cc-pVTZ; $\omega_e(N_2)/\text{cc-pVTZ} = 2345.5 \text{ cm}^{-1}$. Severe technical problems hampered the calculation of the harmonic frequencies for the linear tetraatomics ScN_2Sc and CrN_2Cr at the RCCSD(T) level of theory.

$$r_\infty: 3d_{z^2}^{1.0} 3d_{xz}^{1.0} 3d_{x^2-y^2}^{1.0} 3d_{yz}^{1.0} 4p_y^{1.0} 3d_{xy}^{1.0} / \text{Cr} 2s^{1.74} 2p_z^{1.22} 2p_x^{0.97} \\ \times 2p_y^{0.97} 3d^{0.10} / N,$$

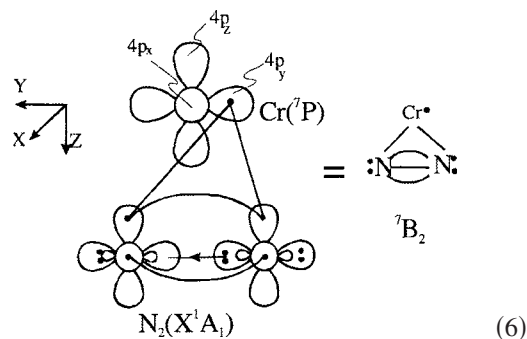
indicate the involvement of the $M_L = \pm 1$ component of the 7F term. The approximately single reference character of the ${}^7\Pi$ state ($\approx 0.94 | 1\sigma^2 2\sigma^2 3\sigma^2 4\sigma^1 1\pi^4 2\pi_x^1 3\pi_x^1 2\pi_y^1 1\delta_x^1 1\delta_y^1 |$) and the r_e populations support the vBL diagram (5).



(Notice that in the diagram above the five $4s^1 3d^2 3d^2$ spectator electrons have been suppressed). The *in situ* Cr atom finds itself in the 7F state, but adiabatically the ${}^7\Pi$ state correlates to the fragments $\text{Cr}({}^7P) + \text{N}_2(X^1\Sigma_g^+)$ (Fig. 4). Through the π_x (or π_y) route, $0.56e^-$ are transferred from Cr to the $-N_2$ moiety, whereas about $0.25e^-$ is back transferred through the σ frame to the metal, leaving it charge deficient by $0.3e^-$.

The RCCSD(T)/ANO+AQZ binding energy is $D_e(\text{Cr}-\text{N}_2) = 27.0$ kcal/mol with respect to the adiabatic products at $r_e = 1.974$ Å.

Now, under C_{2v} symmetry constraints, the ${}^7\Pi^+$ state splits into two T-shaped states of 7B_1 and 7B_2 symmetries, plus one 7A_1 state related to the $M_L = 0$ vector component of the $\text{Cr}({}^7P)$ atom, i.e., to the ${}^7\Sigma^+$ state; see vBL diagram (6).



By moving the “outer” electron from the $4p_y$ atomic orbital (7B_2) to the $4p_x$ or $4p_z$ orbitals, the 7B_1 and 7A_1 states are obtained. Our calculations indicate that the latter one is repulsive as expected. However, the 7B_2 state is bound by 25.4 (19.6) [22.3] kcal/mol with respect to the $\text{Cr}({}^7P) + \text{N}_2$ fragments at the RCCSD(T) (MRCI) [MRCI+Q] level of theory, the result of a $3e^-$ -3 orbital bond (see also the relevant vBL diagram (2) of ScN_2 1^4B_1 state with $D_e = 23.2$ (16.6) [18.7] kcal/mol). In total, about $0.5e^-$ are transferred from the metal to N_2 according to the MRCI atomic Mulliken populations. In detail

$$4s^{0.25} 4p_z^{0.08} 3d_{z^2}^{0.90} 3d_{xz}^{1.0} 4p_x^{0.03} 3d_{yz}^{0.98} 4p_y^{0.20} 3d_{x^2-y^2}^{0.99} 3d_{xy}^{0.99} / \text{Cr} \\ \times 2s^{1.72} 2p_z^{1.33} 2p_x^{0.95} 2p_y^{1.16} 3d^{0.1} / N.$$

On the other hand, the 7B_1 state is only weakly bound, $D_e = 2.8$ kcal/mol, the result of a slight electron transfer from the π_z system of N_2 to the empty $4p_z$ orbital of the Cr atom.

V. THE TETRATOMICS M_2N_2 , $M=\text{Sc, Ti, V, AND Cr}$

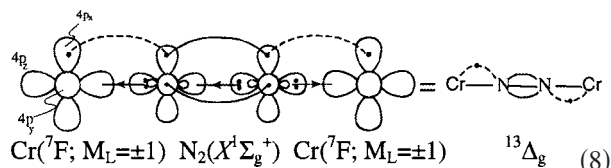
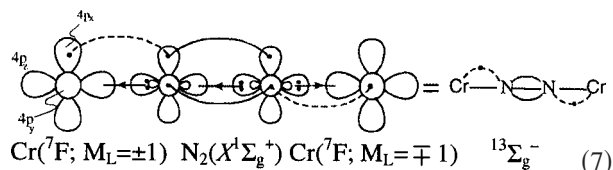
A. Linear

In the introductory section it was mentioned that the linear high-spin tetratomics $M \leftarrow \text{N} \equiv \text{N} \rightarrow M$, $M=\text{Sc, Ti, V, and Cr}$ should be bound with respect to the relevant excited states of the M atoms and with binding energies about twice as large as compared to the parent triatomics, see diagrams (1) and (2). It is also expected for reasons already discussed (see also Ref. 1) that the bond length of $MN-NM$ should increase substantially versus the triatomics and of course relatively to the free $\text{N}_2(X^1\Sigma_g^+)$. To test these thoughts we have examined at the RCCSD(T), C-RCCSD(T), and C-RCCSD(T)+DKH2/ANO+AQZ levels the septet, nonet, and undecet states of spatial symmetries Σ_u^+ , Γ_g , and Σ_u^+ of the centrosymmetric species ScN_2Sc , TiN_2Ti , and VN_2V , respectively; the high-spin linear tetratomic CrN_2Cr will be examined separately. Our results are reported in Table III.

Indeed, binding energies with respect to $2M+\text{N}_2$ conform admirably to our expectations: At the highest level of computation [C-RCCSD(T)+DKH2], twice the $M-\text{N}_2$ binding energy of the triatomic is within a range of ± 1 kcal/mol per bond of $M-\text{N}_2-M$. With the exception of the ${}^7\Sigma_u^+$ state of ScN_2Sc at the RCCSD(T) level, where the $\text{Sc}-\text{N}_2-\text{Sc}$ dissociation energy is 7.1 kcal/mol higher than twice the $\text{Sc}-\text{N}_2({}^4\Sigma^-)D_e$ value, the same holds true for all methods of calculation and for the three MN_2M systems, $M=\text{Sc, Ti, V}$.

Equilibrium $M-\text{N}_2$ bond distances of the tetratomics are all larger than the corresponding triatomics in all methods of calculation, with differences ranging from 0.003 Å [$\text{ScN}_2\text{Sc}/\text{RCCSD(T)}$] to 0.046 Å [$\text{TiN}_2\text{Ti}/\text{C-RCCSD(T)+DKH2}$]. Finally, it is interesting to contrast the N-N bond length differences of the triatomics ($MN-N$) and tetratomics ($MN-NM$) with respect to the free N_2 molecule, Δr_1 and Δr_2 , respectively. At the RCCSD(T)/[C-RCCSD(T)+DKH2]/ANO+AQZ level we obtain $\Delta r_1/\Delta r_2$ (Å) = 0.057/0.135 [0.048/0.100], 0.034/0.061 [0.032/0.051], and 0.015/0.030 [0.015/0.029] for $\text{ScN}_2({}^4\Sigma^-)/\text{ScN}_2\text{Sc}({}^7\Sigma_u^+)$, $\text{TiN}_2({}^5\Delta)/\text{TiN}_2\text{Ti}({}^9\Gamma_g)$, and $\text{VN}_2({}^6\Sigma^+)/\text{VN}_2\text{V}({}^{11}\Sigma_u^+)$, respectively, i.e., $\Delta r_2 \approx 2(\Delta r_1)$ for both methods and the three couples of molecules, see Tables II and III. The seven harmonic frequencies for the two linear tetratomics TiN_2Ti and VN_2V are real, therefore ensuring their stability with respect to vibrational motions (Table III). For the ScN_2Sc we were unable to calculate the harmonic frequencies due to severe technical problems, but we presume that they are real as well.

The interaction of CrN_2 ${}^7\Pi$ state with $\text{Cr}({}^7P)$ in a linear fashion gives rise to two high-spin (tridecet) states of symmetry ${}^{13}\Sigma_g^-$ and ${}^{13}\Delta_g$ as shown in the vbL diagrams (7) and (8) (the $4s^1 3d^2 3d^2$ electrons of each Cr atom are suppressed).

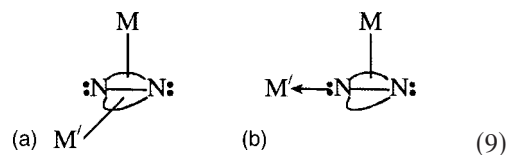


The two states are practically degenerate, with the ${}^{13}\Sigma_g^-$ state being formally the lowest by 0.72 kcal/mol. The binding energies (D_e) with respect to $2\text{Cr}({}^7P)+\text{N}_2(X^1\Sigma_g^+)$ are 56.0 and 55.2 kcal/mol for the ${}^{13}\Sigma_g^-$ and ${}^{13}\Delta_g$ states, respectively, two times larger than the D_e value of the parent ${}^7\Pi$ state of the linear triatomic CrN_2 , whose D_e value is 27.0 kcal/mol with respect to $\text{Cr}({}^7P)+\text{N}_2$ (Tables II and III).

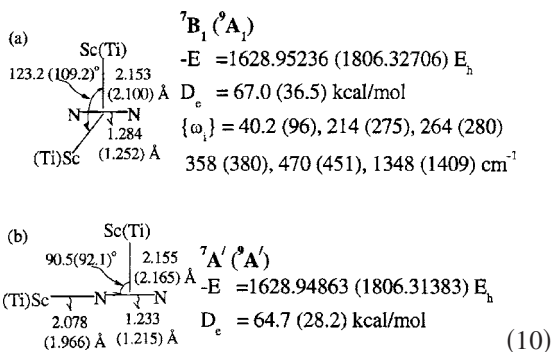
To conclude this section we should mention that as early as 1991 and 1993, Siegbahn¹⁴ and Blomberg and Siegbahn¹⁵ examined the side-on interaction of $M_2\text{N}_2$ species, where $M=\text{Ti, Cr, Fe, Co, and Ni}$ (Ref. 14) and Ti, Y, Zr, and Nb (Ref. 15) employing the averaged coupled-pair functional (ACPF) and modified coupled-pair functional (MCPF) methods, respectively, with a $[5s4p3d/M3s2p1d/N]$ basis set. Their conceptual approach is considerably different than ours and conclusive comparisons with the present work is very difficult at least for the Ti_2N_2 and Cr_2N_2 species.

B. Nonlinear (C_{2v} , C_s)

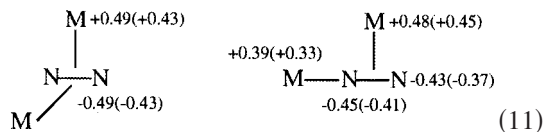
We remind that for the nonlinear T-shaped triatomics ScN_2 (4B_1) and TiN_2 (5A_1), the RCCSD(T)/ANO+AQZ binding energies are 23.2 and 8.5 kcal/mol, respectively (Table II). Within the spirit of vbL diagram (2) and the discussion of Sec. IV A, two high-spin geometrical configurations of nonlinear tetratomics Sc_2N_2 and Ti_2N_2 are expected to be significantly bound with respect to the first excited states of $2\text{Sc}({}^4F)$ and $2\text{Ti}({}^5F)+\text{N}_2(X^1\Sigma_g^+)$, namely,



$M, M'=\text{Sc, Ti}$. Of course, in diagram (9b) exchanging the M, M' atoms a different isomer is obtained. Here we limit ourselves to the $M=M'$ species, therefore spatial symmetry C_{2v} in diagram (9a). Complete RCCSD(T)/ANO+AQZ optimization under C_{2v} (9a) and C_s (9b) constraints gives the results displayed in diagrams (10a) and (10b). Limitations of our computing resources did not allow us to calculate harmonic frequencies for the (9b) case.



Observe that (a) the C_{2v} molecules are lower in energy than the corresponding C_s by 2.3 and 8.3 kcal/mol for Sc_2N_2 and Ti_2N_2 , respectively. (b) Both the C_{2v} $\text{Sc}_2\text{N}_2({}^7B_1)$ and $\text{Ti}_2\text{N}_2({}^9A_1)$ species are lower in energy from their linear counterparts ${}^7\Sigma_u^+$ and ${}^9\Gamma_g$ by 17.1 and 8.1 kcal/mol. (c) The C_s $\text{Sc}_2\text{N}_2({}^7A')$ is also more stable than the linear ${}^7\Sigma_u^+$ one by 14.8 kcal/mol, but $\text{Ti}_2\text{N}_2({}^9A')$ and $\text{Ti}_2\text{N}_2({}^9\Gamma_g)$ are practically degenerate; see Table III. (d) Although our Mulliken gross charges being at the Hartree-Fock level are rather exaggerated, yet the observed trends are in relative accord with the MRCI populations of the corresponding T-shaped and linear triatomics [diagram (11)].



In all cases a total of (0.8-1.0) e^- are migrating from the Sc and Ti atoms to the N_2 molecule, resulting to a considerable increase of the $-\text{N}\equiv\text{N}-$ bond length with respect to the free $\text{N}_2(X^1\Sigma_g^+)$, ranging from 0.114 ($\text{Ti}_2\text{N}_2, C_s$) to 0.183 ($\text{Sc}_2\text{N}_2, C_{2v}$). Interestingly, the extension of the $-\text{N}\equiv\text{N}$ bond in all cases is practically additive with respect to the corresponding triatomics. For instance, in the T-shaped and linear $\text{Sc}_2\text{N}_2({}^4B_1, {}^4\Sigma^-)$, the $\Delta r_e(-\text{N}\equiv\text{N}-)$ upon bonding is 0.078 and 0.057 Å, whereas in the relevant tetraatomics $\text{Sc}_2\text{N}_2({}^7B_1, {}^7A')$ is 0.183 [$\approx 2(0.078)$] and 0.132 ($\approx 0.078 + 0.057$) Å, respectively [Table II and diagrams (10a) and (10b)]. (e) Finally, all binding energies (or “atomization” energies with respect to the three entities $2M[\text{Sc}({}^4F), \text{Ti}({}^5F)] + \text{N}_2$ are considerably larger than the sum of the binding energies of the relevant triatomics, T shaped or linear.

VI. SUMMARY AND REMARKS

Using coupled-cluster and multireference variational methods in conjunction with large to very large basis sets, we have studied the interaction of the early 3d transition metals $M = \text{Sc}, \text{Ti}, \text{V}$, and Cr with $\text{N}_2(X^1\Sigma_g^+)$. In particular, we have focused on the high-spin triatomics ($M\text{N}_2$) and tetraatomics ($M_2\text{N}_2$) linear or not. For selected states of the $M\text{N}_2$ molecules potential energy profiles have been constructed at the RCCSD(T) level. We report geometries, bond energies, harmonic frequencies, and dipole moments. Our main inferences are the following.

- (i) Considering the “inertness” of the N_2 molecule, the $M + \text{N}_2$ (or $2M + \text{N}_2$) attractive interactions can be

TABLE IV. Comparison of dissociation energies $D_e(M-X)$ and equilibrium bond lengths $r_e(M-X)$ of the linear triatomics MX ($X = \text{N}_2, \text{CO}$). In parenthesis are results from Ref. 5: DFT (B3LYP)/[6-311+G(2d,p)].

Molecule	D_e^a (kcal/mol)	r_{M-X} (Å)
$\text{ScN}_2({}^4\Sigma^-)$	22.0(35.0)	2.024(2.096)
$\text{ScCO}({}^4\Sigma^-)^b$	37	2.080
$\text{TiN}_2({}^5\Delta)$	13.8(30.2)	2.001(2.009)
$\text{TiCO}({}^5\Delta)^b$	28	2.033
$\text{VN}_2({}^6\Sigma^+)$	7.8(22.4)	2.024(1.978)
$\text{VCO}({}^6\Sigma^+)^b$	19	2.00
$\text{CrN}_2[{}^7\Sigma^+({}^7A')]$	repulsive (13.3)	\cdots (2.117)
$\text{CrCO}[{}^7\Sigma^+({}^7A')^b]$	~ 2	2.18

^a D_e with respect to $\text{Sc}({}^4F), \text{Ti}({}^5F), \text{V}({}^6D)$, and $\text{Cr}({}^7S) + \text{N}_2(X^1\Sigma_g^+)$.

^bReference 1.

characterized as significant, ranging from about 10 to 30 (or 30 to 70) kcal/mol.

- (ii) In Table IV we contrast binding energies and bond distances of the linear triatomics $M\text{N}_2$ and $M\text{CO}$;¹ for reasons of comparison recent results on the $M\text{N}_2$ species at the DFT level are also displayed.⁵ Two observations are clear: (a) for both $M\text{N}_2$ and $M\text{CO}$ systems, the binding energies decrease monotonically from Sc to Cr, and (b) the DFT approach gives completely different $M-\text{N}_2$ (and $M-\text{CO}$, see Ref. 1) dissociation energies in comparison with the present *ab initio* results. It is also of interest at this point to compare the dissociation energies of $M\text{CO}$ species at DFT(BPW91/6-311+G*)¹⁶ and DFT[B3LYP/6-311G(2d)]¹⁷ approaches in relation to the *ab initio* values of Table IV: 29.7, 35.5, 33.0, and 9 kcal/mol (Ref. 16, D_0) and 49.7, 45.3, 26.6, and 5.8 kcal/mol (Ref. 17, D_e), for $\text{ScCO}({}^4\Sigma^-)$, $\text{TiCO}({}^5\Delta)$, $\text{VCO}({}^6\Sigma^+)$, and $\text{CrCO}({}^7A')$, respectively.
- (iii) Ground state fragments M and N_2 give rise to repulsive states.
- (iv) All bound molecular states correlate to the first excited states of $\text{Sc}({}^4F), \text{Ti}({}^5F), \text{V}({}^6D)$, and the sixth excited state of $\text{Cr}({}^7P)$. The bonding in the linear $M\text{N}_2$ species is due to σ charge donation from N_2 to M , with synchronous M to N_2 “back donation” through the π -conjugated route, very similar to the isoelectronic species $M\text{CO}$.¹ For the T-shaped (C_{2v}) triatomics the bonding can be attributed to $3d(M) - 2p(\text{N}-\text{N})$ interactions on the plane of the molecule [see diagram (2)]. In tetraatomics, linear ($D_{\infty h}$) or not (C_{2v}/C_s), the binding mechanism is completely analogous to the corresponding parental triatomics.

ACKNOWLEDGMENTS

Two of the authors (C.K. and S.K.) express their gratitude to the Hellenic State Scholarship Foundation (IKY) for financial support. A.M. is grateful to the EPEAEK program PYTHAGORAS (Grant No. 70/3/7373) for basic research.

¹C. Koukounas, S. Kardahakis, and A. Mavridis, J. Chem. Phys. **123**, 074327 (2005).

²P. E. Siegbahn and M. R. A. Blomberg, Chem. Rev. (Washington, D.C.)

- 100**, 421 (2000), and references therein.
- ³L. Andrews, W. D. Bare, and G. V. Chertihin, *J. Phys. Chem. A* **101**, 8417 (1997).
- ⁴G. V. Chertihin, L. Andrews, and C. W. Bauschlicher, Jr., *J. Am. Chem. Soc.* **120**, 3205 (1998).
- ⁵J. Pilme, B. Silvi, and M. E. Alikhani, *J. Phys. Chem. A* **109**, 10028 (2005).
- ⁶C. A. Moore, *Atomic Energy Levels*, Natl. Bur. Stand. Ref. Data Ser., Natl. Bur. Stand. Circ. No 35 (U.S. GPO, Washington D.C., 1971).
- ⁷K. P. Huber and G. Herzberg, *Constants of Diatomic Molecules* (Van Nostrand Reinhold, New York, 1979).
- ⁸C. W. Bauschlicher, Jr., *Theor. Chim. Acta* **92**, 183 (1995).
- ⁹T. H. Dunning, Jr., *J. Chem. Phys.* **90**, 1007 (1989); R. A. Kendall, T. H. Dunning, Jr., and R. J. Harrison, *ibid.* **96**, 6796 (1992).
- ¹⁰N. B. Balabanov and K. A. Peterson, *J. Chem. Phys.* **123**, 064107 (2005).
- ¹¹H.-J. Werner, P. J. Knowles, R. D. Amos *et al.*, *MOLPRO 2000, version 2002.6*, Birmingham, 1999.
- ¹²P. J. Knowles, C. Hampel, and H.-J. Werner, *J. Chem. Phys.* **99**, 5219 (1993); *J. Chem. Phys.* **112**, 3106 (2000); M. J. O. Deegan and P. J. Knowles, *Chem. Phys. Lett.* **227**, 321 (1994).
- ¹³M. Douglas and N. M. Kroll, *Ann. Phys. (N.Y.)* **82**, 89 (1974); B. A. Hess, *Phys. Rev. A* **32**, 756 (1985); **33**, 3742 (1986).
- ¹⁴P. E. M. Siegbahn, *J. Chem. Phys.* **95**, 364 (1991).
- ¹⁵M. R. A. Blomberg and P. E. M. Siegbahn, *J. Am. Chem. Soc.* **115**, 6908 (1993).
- ¹⁶G. L. Gutsev, L. Andrews, and C. W. Bauschlicher, Jr., *Chem. Phys.* **290**, 471 (2003).
- ¹⁷J. Pilme, B. Silvi, and M. E. Alikhani, *J. Phys. Chem. A* **107**, 4506 (2003).